# University of Groningen

## High-Throughput Screening and Hierarchical Topography-Mediated Neural Differentiation of Mesenchymal Stem Cells
Yang, Liangliang; Jurczak, Klaudia Malgorzata; Ge, Lu; van Rijn, Patrick

**IMPORTANT NOTE: You are advised to consult the publisher's version (publisher's PDF) if you wish to cite from it. Please check the document version below.**

*Document Version*
Publisher's PDF, also known as Version of record

[Link to publication in University of Groningen/UMCG research database](Link to publication in University of Groningen/UMCG research database)

FULL PAPER

ADVANCED
HEALTHCARE
MATERIALS

www.advhealthmat.d

Check for
updates

# High-Throughput Screening and Hierarchical Topography-Mediated Neural Differentiation of Mesenchymal Stem Cells

*Liangliang Yang, Klaudia Malgorzata Jurczak, Lu Ge, and Patrick van Rijn\**

**Biophysical factors such as anisotropic topography composed of micro/nano-sized structures are important for directing the fate of human bone marrow-derived mesenchymal stem cells (hBM-MSCs) and have been applied to neuronal differentiation. Via high-throughput screening (HTS) methods based on topography gradients, the optimum topography is determined and translated toward a hierarchical architecture designed to mimic the nerve nano/microstructure. The polydimethylsiloxane (PDMS)-based topography gradient with amplitudes (_A_) from 541 to 3073 nm and wavelengths (_W_) between 4 and 30 µm is developed and the fate commitment of MSC toward neuron lineage is investigated. The hierarchical structures, combining nano- and microtopography (W0.3/W26 parallel/perpendicular) are fabricated to explore the combined topography effects on neuron differentiation. From the immunofluorescent staining results (Tuj1 and MAP2), the substrate characterized by _W_: 26 µm; _A_: 2.9 µm shows highest potential for promoting neurogenesis. Furthermore, the hierarchical features (W0.3/W26 parallel) significantly enhance neural differentiation. The hBM-MSCs on the hierarchical substrates exhibit a significantly lower percentage of nuclear Yes-associated protein (YAP)/TAZ and weaker cell contractility indicating that the promoted neurogenesis is mediated by the cell tension and YAP/TAZ pathway. This research provides new insight into designing biomaterials for applications in neural tissue engineering and contributes to the understanding of topography-mediated neuronal differentiation.**

## 1. Introduction

Neural regeneration aiming at repairing the central nervous system, including brain and spinal cord injury, poses great challenges in the clinic.[1] To overcome this, directed differentiation of stem cells into neurons has been developed for cell replacement therapy.[2–5] Stem cells are undifferentiated cells with self-renewal capacity and the ability to differentiate into multiple cell types,[6] for instance, osteogenic,[7] adipogenic,[8] chondrogenic,[9] and neurogenic[10] lineages, which hold tremendous promise for the field of regenerative medicine.[11] Therefore, precise control over the differentiation process is critical for the development of therapeutic approaches.[12] Previous research has shown that, in natural stem cell niche, the biophysical properties of extracellular matrix, e.g., topography,[13–18] stiffness,[19–22] elasticity[23,24] and bioelectricity,[25,26] have sophisticated influence on the behavior of stem cells, including their adhesion, self-renewal, migration, and differentiation.[27,28] The surface topography significantly affects cell morphology, spreading, and orientation through a phenomenon known as contact guidance.[29] Cells sense such surface patterns ranging from 10 nm to 100 µm.[30,31]

There are many studies focused on the neuron differentiation of stem cells mediated by topography. For example, Yim and co-workers[32–34] have developed a multi-architecture chip (MARC) array consisting of isotropic and anisotropic features, in nano- to micrometer dimensions to investigate the influence of different geometries and sizes in neural differentiation. Chi and co-workers[35] investigated the effect of nanograting substrates with different widths (width: 350 nm/2 mm/5 mm, height: 300 nm) on human-induced pluripotent stem cells development toward neuronal lineage. They found that a width of 350 nm induced the highest neuronal marker expression. However, most of these studies focused on independent substrates with randomly selected parameters, which provided interesting yet limited information. To date, there are relatively few studies devoted to the investigation of the high-throughput screening (HTS) of topography on neural differentiation. Im and co-workers[36] developed a series of anisotropic wrinkle structures with a range of wavelength (from 50 nm to 37 µm), and found two distinct characteristic length regions (100 nm and the wavelengths larger than 1.4 µm) that enhanced the neuron differentiation. However, in their study, the wavelength parameters were not altered in a continuous way, thereby providing interesting but incomplete information.

L. Yang, K. M. Jurczak, L. Ge, Dr. P. v. Rijn
Department of Biomedical Engineering
University Medical Center Groningen
University of Groningen
Groningen, A. Deusinglaan 1, Groningen 9713 AV, The Netherlands
E-mail: p.van.rijn@umcg.nl

The ORCID identification number(s) for the author(s) of this article can be found under https://doi.org/10.1002/adhm.202000117.

**ADVANCED
SCIENCE NEWS**
www.advancedsciencenews.com

**ADVANCED
HEALTHCARE
MATERIALS**
www.advhealthmat.de

High-throughput screening has the ability to scale up the number of interested samples, allowing the simultaneous analysis of numerous important parameters including biophysical and (bio)chemical factors,[37] and the optimum parameter is screened at last. Topography and stiffness gradients offer an ideal platform to address the advantage of high-throughput screening on cell behavior.[38] This platform allows systematic studies to be performed with a continuously varying surface parameter, so there is hundreds or even thousands of material parameters in a single substrate. Moreover, it is time and cost-efficient and minimizes systematic or methodological errors.[39] Previously, our group utilized micro/nanotopographical gradients for studying cell contact guidance and found that human bone marrow-derived mesenchymal stem cells (hBM-MSCs) alignment, elongation, cytoskeleton arrangement, filopodia development as well as cell adhesion significantly depended on the parameter of topography.[38,40] Additionally, we found that topography-induced cell behavior greatly depends on the cell type, and the differentiation of satellite cells toward skeletal muscle had a positive stimulus originating from different topography dimensions than that MSCs do.[41–44]

In addition, it is important to note that the ECM architecture of nerve tissue in vivo is composed of complex and anisotropically hierarchical structure with various sizes ranging from nanometers to micrometers that interacts with cells and regulates their behavior and fate.[45] This hierarchical structure could induce stem cell differentiation through the interaction between cells and micro- and nanostructured surfaces.[12] Microscale cues induce morphological changes, direct the rearrangement of the cytoskeleton, alter the shape of the nucleus, and modulate-related gene expression.[46] Nanoscale cues can promote the clustering of integrins, followed by the activation of the integrin-mediated intracellular signaling pathway and in turn regulates stem cell differentiation.[47] However, there are few studies reporting spatial control of neuron differentiation of stem cells using topographies with different spatial dimensions ranging from nanometers to micrometers due to difficulties in the preparation of such hierarchical structures on a single substrate and use arbitrary features without any optimization approaches.

The research question we aimed to address is "Do combined nano- and microtopography enhance the neuronal differentiation?" Rather than utilizing arbitrarily chosen features, we firstly identified the optimum microtopography features by developing an aligned PDMS-based topography (wrinkle) gradient (Wavelength range from 4 to 30 μm, and amplitude range from 541 to 3073 nm) to systematically investigate the effect on the commitment of hBM-MSCs toward neuron lineage differentiation. Moreover, the optimum microtopography for neurogenesis was identified and further combined with the previously identified nanotopography to stimulate different pathways simultaneously. The differentiation behavior was analyzed by different markers (Tuj1 and MAP2 for neurons, GFAP for astrocytes) after culturing cells for the different time periods (7, 14, and 21 d). The workflow is shown in **Figure 1**. Furthermore, the combined effect of nanosized and microsized topography was investigated utilizing hierarchical wrinkled structures where the orientation of the nanotopography with respect to
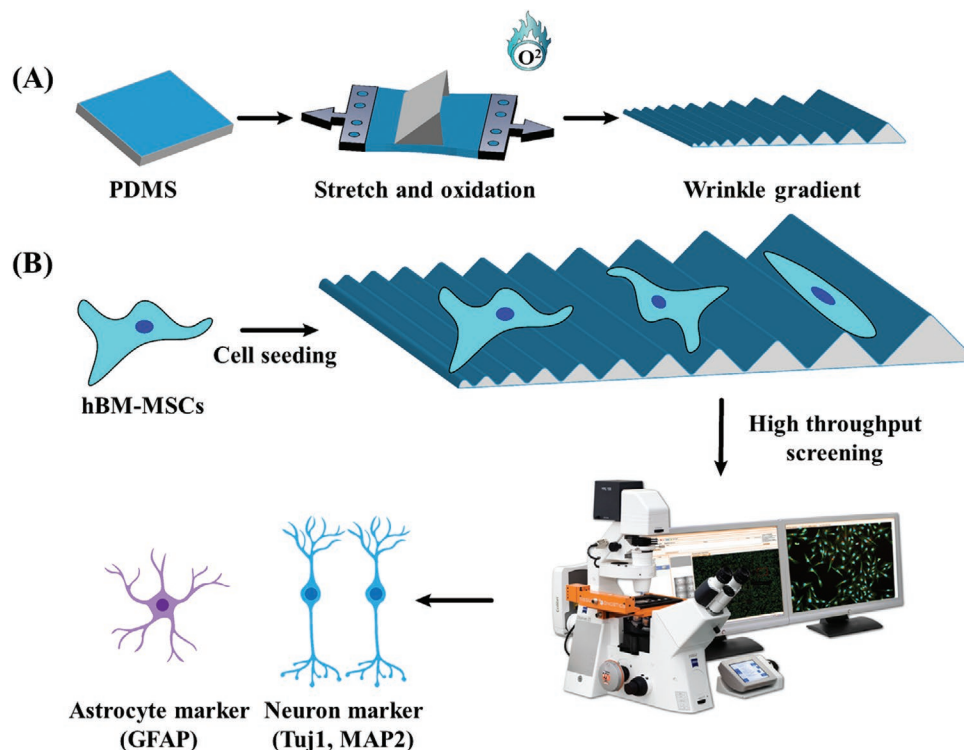


**Figure 1.** Schematic representation of the screening platform for neuron differentiation. A) Wrinkle gradient was prepared by the shielded plasma oxidation. B) The workflow of the differentiation process. hBM-MSCs were cultured on wrinkle gradient for 7, 14, and 21 d to induce neurogenesis. The differentiation behavior was analyzed by immunofluorescent staining with different markers (Tuj1 and MAP2 for neurons, GFAP for astrocytes, respectively) and further imaged with TissueFaxs.

**ADVANCED
SCIENCE NEWS**
www.advancedsciencenews.com

**ADVANCED
HEALTHCARE
MATERIALS**
www.advhealthmat.de

the microtopography was varied. Intriguingly, the hierarchical structure showed enhanced neurogenesis in comparison to single-scale structures and the orientation of both features with respect to one another tremendously affected the differentiation potential. Besides, to understand the underneath mechanism, cell contractility and Yes-associated protein (YAP)–TAZ localization were characterized by immunofluorescent staining. Taken together, this finding enables us to understand the wrinkle size dependency of mechanosensitive neural differentiation but also provides a new insight into the rational design of scaffolds for neural tissue engineering.

## 2. Results

### 2.1. Surface Characterization of Wrinkle Gradient

For the preparation of the topography gradient, PDMS was uniaxially stretched and plasma oxidized. The surface was shielded with a right-angled triangular prism mask to create an oxidation gradient that translates to different topographies upon release of the applied strain. After releasing the strain, a stable wrinkled topographic gradient was generated, which is tunable as a function of plasma time, angle of mask and operating pressure.[38] It has to be noted that, to exclude variations in chemical composition and mechanical properties due to the varied intensity of plasma along the mask area, the PDMS wrinkle gradient was applied as a mold. After that, a fresh mixture of elastomer base/crosslinker was applied on top of the molds. This imprinting approach led to a PDMS wrinkle gradient with different topographies but exhibiting the same surface chemistry and mechanical properties.

The topography gradients were characterized by atomic force microscopy (AFM). Measurements were acquired between 0 and 11.8 mm with equal intervals. The wrinkle size increased from the least exposed side (close side of the mask) to the most exposed side (open side of the mask). The unidirectional gradients were obtained in a highly reproducible manner with amplitudes ($A$; nm) ranging from 541 to 3073 nm and wavelengths ($W$; μm) between 4 and 30 μm as shown in **Figure 2**A,B. Both the amplitude and wavelength displayed a continuous gradual change and provides the means to study topography-driven neuronal differentiation of MSCs.

### 2.2. Effect of Wrinkle Gradient on Neuronal Differentiation of hBM-MSCs

Having established the wrinkle gradient with controlled wavelengths and amplitudes, we investigated the topography-driven fate commitment of hBM-MSCs toward the neural lineage using the topography gradient. For this purpose, the fate commitment of hBM-MSCs cultured on the wrinkle gradient structure was monitored by immunostaining for neural lineage markers (Tuj1, MAP2) and astrocytic lineage marker (GFAP) for different days of cell incubation (7, 14, and 21 d), and Flat surface was used as a control.

The immunodetection of Tuj1, an early marker of the neural differentiation process in undifferentiated MSCs, is shown in

**Figure 3**. The image shows the relative expression of Tuj1 along the wrinkle gradient and Flat surface at day 7 (Figure 3A) and day 14 (Figure 3D). It is clearly seen that the intensity of Tuj1 was gradually increased along the wrinkle gradient. The magnification is shown in Figure 3B,E. Interestingly, the intensity of Tuj1 expression for cells cultured on Flat surface was very low, indicating that the anisotropic wrinkle structure enhances the neuron differentiation compared to a Flat substrate. To further confirm this enhancement, the intensity of Tuj1 expression was quantified (Figure 3C for 7 d and Figure 3F for 14 d) and correlated well with the qualitative analysis. With the increase of wrinkle size, the intensity of Tuj1 gradually increased, and the peak expression of normalized TUJ1 was found at the 10th position (Wavelength: 26.7 μm, amplitude: 2.89 μm) of the wrinkle gradient. Tuj1 intensity for the position of 10th was 30 times and 4.3 times higher for 7 and 14 d, respectively, than that for cells cultured on Flat surface. The difference in relative increase of TUJ1 expression between 7 and 14 d compared to the Flat control is attributed to the still increasing expression of TUJ1 on the Flat substrate while the absolute increase on the wrinkled substrates was not increasing much anymore. These results indicate that hBM-MSCs are sensitive to the wrinkle features and, and a larger wrinkle size is beneficial for neuron differentiation as illustrated by a higher expression of relevant markers at an earlier timepoint.

To test this further, the immunodetection of MAP2, the late marker of the neural differentiation process, was also performed. As shown in **Figure 4**A, the intensity for MAP2 at day 7 on the wrinkle gradient and Flat surface were subtle and not visible, probably because the culture time was not long enough to stimulate the expression of MAP2 as it is a late marker. MAP2 staining for hBM-MSCs cultured for 14 d (Figure 4B) and 21 d (Figure 4E) showed that the expression of MAP2 progressively increased along the wrinkle gradient. The magnifications are shown in Figure 4C,F for 14 and 21 d, respectively. The quantification of the normalized MAP2 is shown in Figure 4D,G. The highest intensity was found at the 10th position of the gradient, which is well consistent with the observation from Tuj1 staining. Compared to Flat surface, a 18 and 11.5 fold increase was observed at the 10th position for 14 and 21 d, respectively.

In addition to Tuj1 and MAP2, the immunostaining of intermediate filament proteins of mature astrocytes (glial fibrillary acidic protein, GFAP) on the wrinkle gradient was shown in Figure S1 (Supporting Information). Importantly, the intensity of GFAP on the wrinkle gradient was not visible for 7, 14, and 21 d. In contrast, there was a slight intensity of GFAP expression on Flat surface for different days (7, 14, and 21 d), indicating that wrinkle structures could suppress hBM-MSCs differentiation into a glial lineage such as astrocytes. In the central nerve system (CNS), astrocytes contribute significantly to the formation of a glial scarring, which creates a barrier to axons.[48] Therefore, the differentiation of stem cells into astrocytes should be suppressed if stem cells are to be used in therapies for spinal cord injury.

In summary, these results indicate that wrinkle size has a significant influence on the neural differentiation, which could be reflected by the varied intensity of neuron markers on the wrinkle gradient. More importantly, the optimum wrinkle
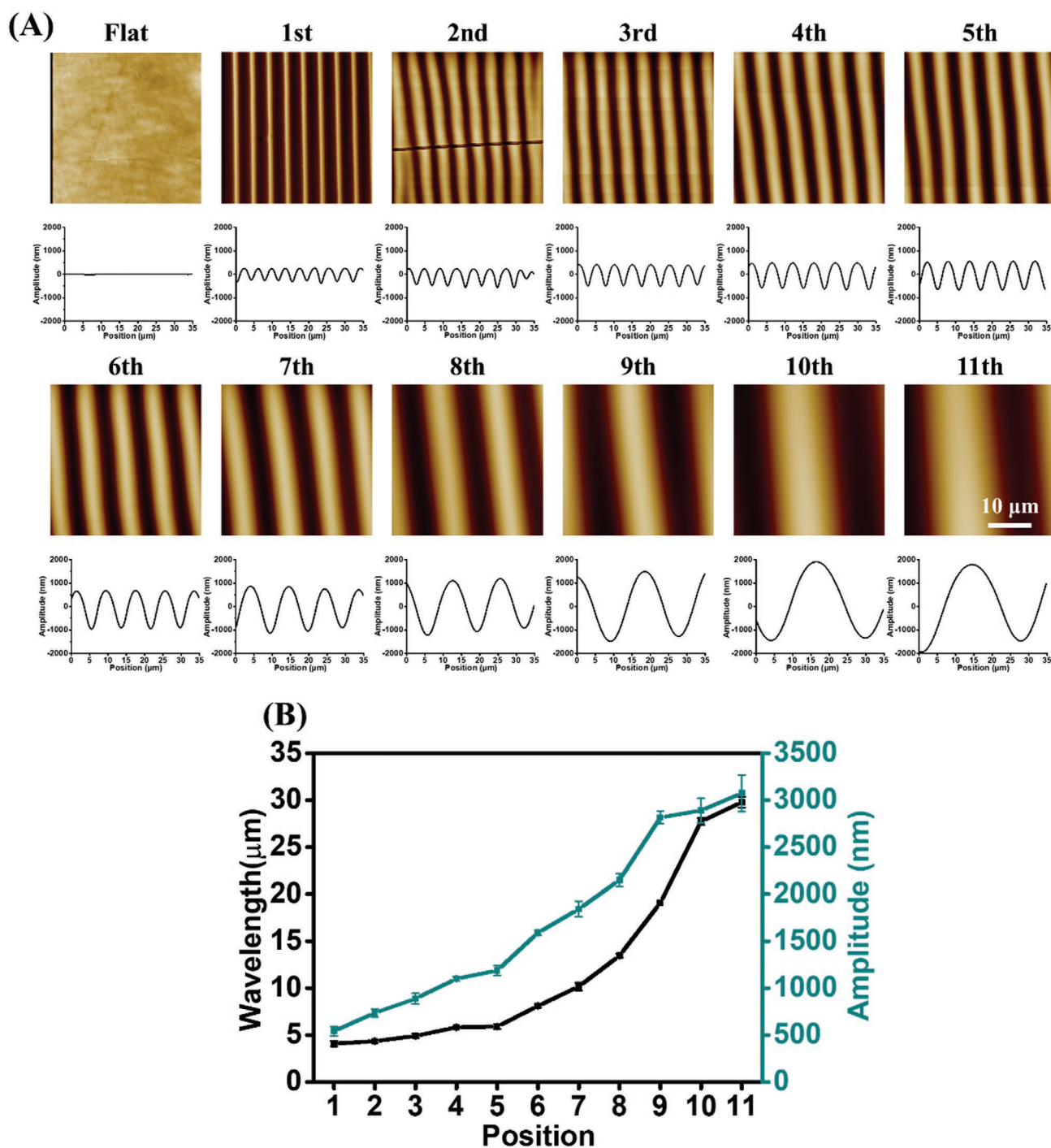
**Figure 2.** A) AFM images and height profiles of wrinkle gradient obtained after imprinting. Flat substrates were obtained under the same conditions without applying the unidirectional strain. Scale bar is 10 µm and applies to all images. B) Quantification of the wavelength and amplitude of the wrinkle gradient. Data are reported as mean ± standard deviation (SD) ($n = 30$ wrinkles, three independent imprints were analyzed).

features for the neurogenesis of stem cell were identified via efficient screening and it was found that wrinkle features with $W$: 26.7 µm A: 2.89 µm supported neuronal differentiation the best. Therefore, W26/A2.9 was selected and prepared as a uniform substrate for further investigations onto which the previously identified nanofeatures are applied to study the combined effects.

## 2.3. Enhanced Neurogenesis by Multiscale Wrinkle Topography

Native ECM of the nerve tissue consists of complex and hierarchical structures with various sizes ranging from nanometers to micrometers.[45] Importantly, there is an ordered anisotropic structure within the tissue. Moreover, some researchers have found that the aligned nanosized geometry is able to guide
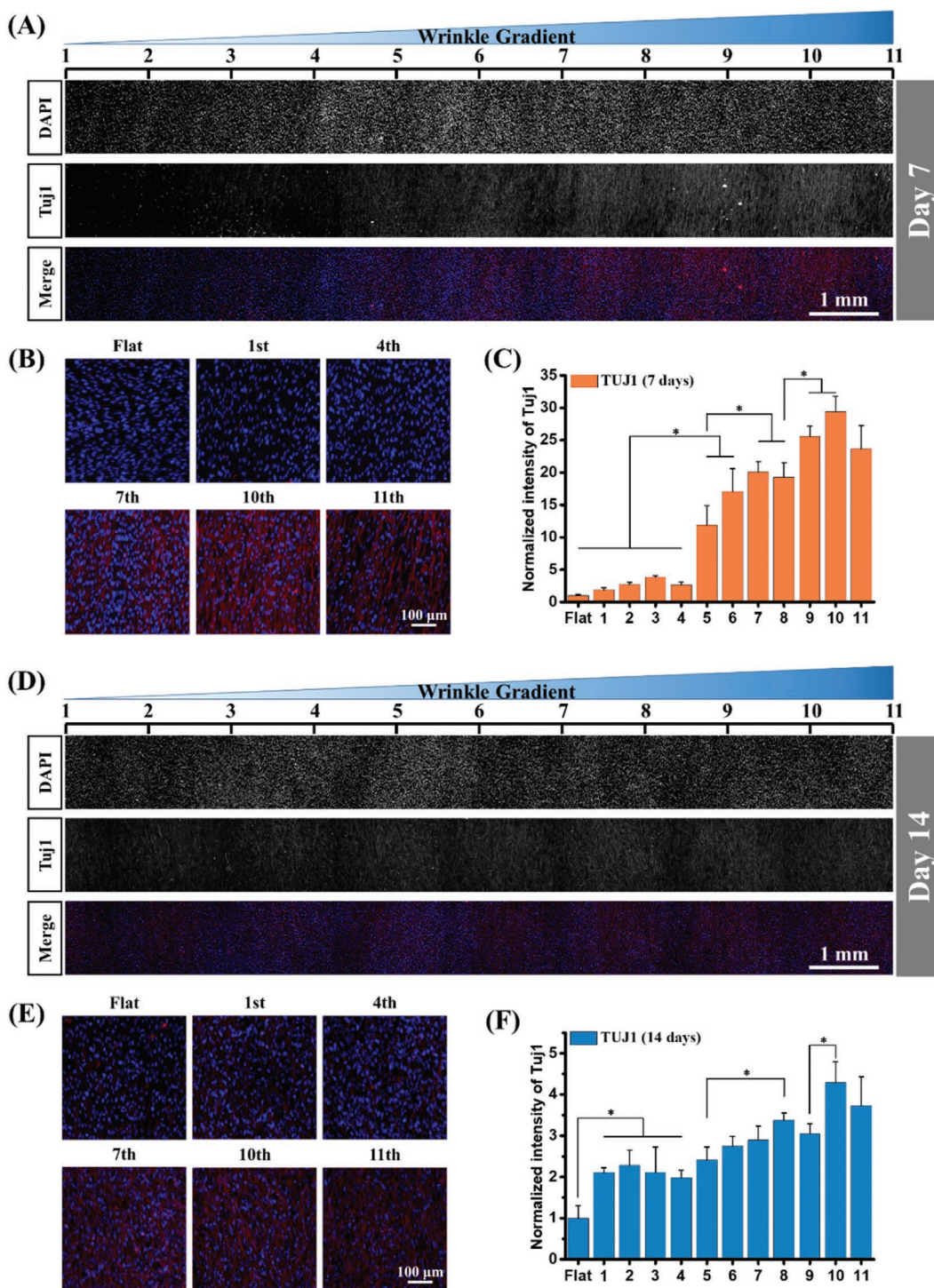
**ADVANCED
SCIENCE NEWS**

www.advancedsciencenews.com

**ADVANCED
HEALTHCARE
MATERIALS**

www.advhealthmat.de

**Figure 3.** Immunodetection of Tuj1 (in red) and nucleus staining (in blue) of cells cultured on wrinkle gradients for A) 7 and D)14 d. Flat surface was used as control. B,E) The magnified image of the representative position. Scale bar represents 1 mm for the gradients and 100 µm for the magnified images. C, F) Quantitative analysis of Tuj1 expression normalized by Flat surface. Data are shown as mean ± standard deviation (SD), and *$P < 0.05$. Each experiment was performed in triplicate.

neural differentiation of stem cells.[48,49] Therefore, we hypothesized that the hierarchical structure composed of different wrinkle sizes (nano- and micro-) may have an enhanced effect on the neural differentiation of hBM-MSCs. A methodology to fabricate micro- and nanostructured hierarchical PDMS substrates with tunable directions was first developed by a combination of sequentially aligned topography preparation via a silicone stretch-oxidation-release method and imprinting lithography.
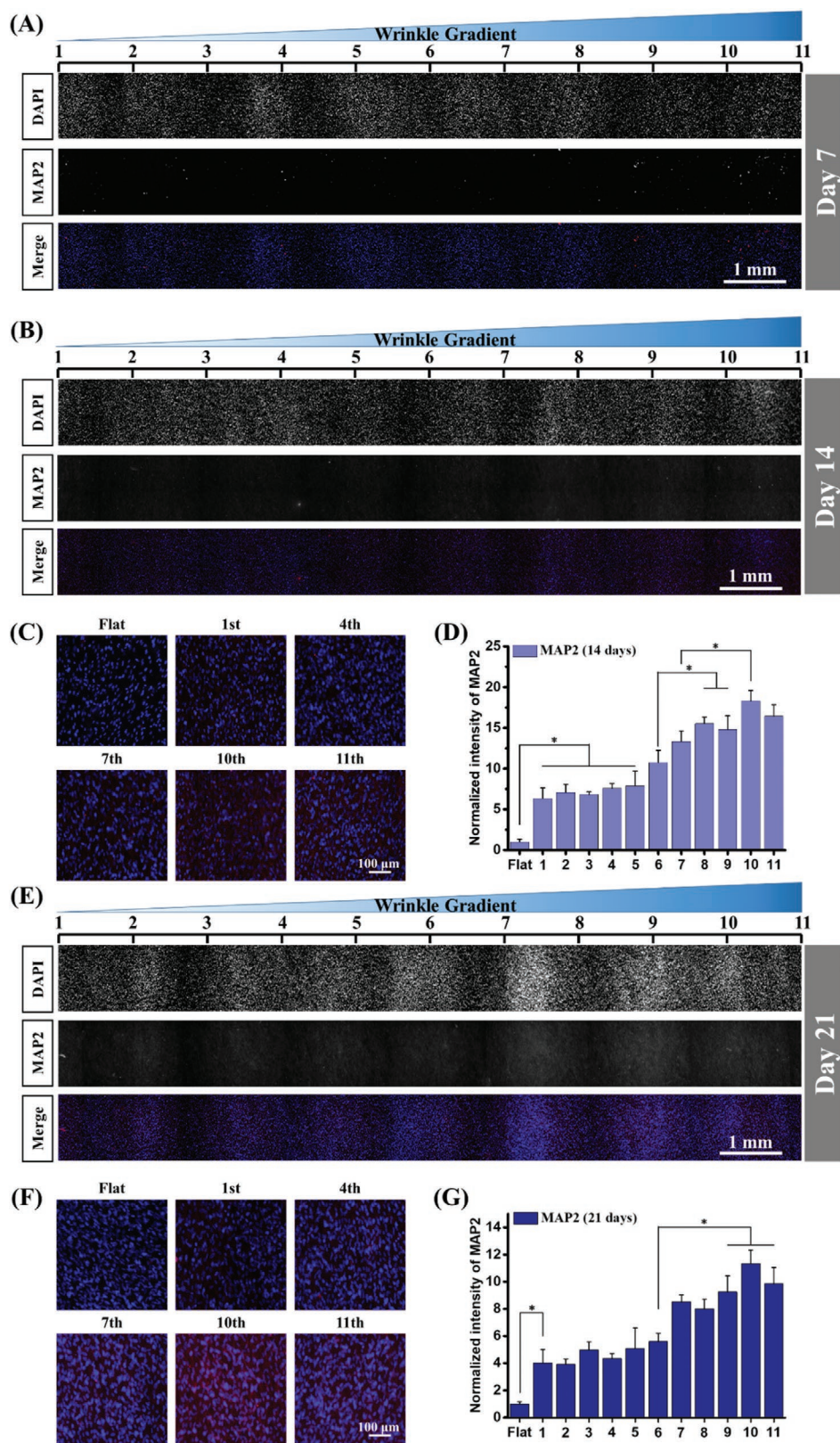
**ADVANCED
SCIENCE NEWS**

www.advancedsciencenews.com

**ADVANCED
HEALTHCARE
MATERIALS**

www.advhealthmat.de

**Figure 4.** Immunodetection of MAP2 (in red) and nucleus staining (in blue) of cells cultured on wrinkle gradients for A) 7, B) 14, and E) 21 d. Flat surface was used as control. C,F) The magnified image of the representative position. Scale bar represents 1 mm for the gradients and 100 μm for the magnified images. D,G) Quantitative analysis of MAP2 expression normalized by Flat surface. Data are shown as mean ± standard deviation (SD), and *$P < 0.01$. Each experiment was performed in triplicate.

After the preparation of the single-scale substrate, the double-scaled hierarchical topography was fabricated. The orientation between newly added and the previous topography was done by controlling the stretching direction. It is important to point out that the addition of a new topography was performed after the preparation of larger feature. Besides, there will be a bioglass-like ($SiO_2$) layer on the surface of substrate after the oxidation, so it is critical that before the preparation of hierarchical substrates, the mold was imprinted into pristine PDMS to obtain a soft substrate with the same topography of mold. This substrate can further be stretched and oxidized to create the hierarchical structure. The angle between the different topographies was varied by controlling the stretching direction of the freshly imprinted substrate (**Figure 5**A,B). Although any angle (orientation) may be chosen, we limited the system here to 0° (parallel) and 90° (perpendicular). In this study, two different scaled hierarchical substrates were prepared: double scale (W0.3 parallel and perpendicular with W26, which was further reported as W0.3∥W26 and W0.3⊥26, respectively), and single scale (Flat, W0.3, and W26).

The surface features were characterized by AFM. As shown in Figure 5C, wave-like topographies (single scale) were achieved with varying dimensions (W0.3A0.02 and W26A2.9). Importantly, for hierarchical structures, W0.3 could be clearly observed on the top of W26. The height profile of the structured PDMS is shown in Figure 5D. Taken together, the AFM results demonstrate that the innovative fabrication method for hierarchical architectures is scalable and tunable, providing multiscaled hierarchical substrates that are able to mimic the structure of nerve tissue.

To investigate the influence of the hierarchical substrates on cell morphology, hBM-MSCs were seeded on the different topographies and allowed to attach and spread for 24 h. To visualize the cell morphology, the actin and nucleus were stained and imaged, respectively. Cell orientation, considered as the percentage of cells that have their major axis within 10° from the direction of the wrinkle, was quantified with Fiji software. As shown in **Figure 6**A, cell morphologies were significantly influenced by the surface topography. Cells grown on Flat and W0.3 had irregular morphology and were randomly oriented (19% and 30%, respectively). In contrast, cells cultured on W26 exhibited a higher degree of orientation (67%) along the direction of the wrinkle, and more elongated shapes. For the hierarchical structures, cells grown on the W0.3∥26 showed the highest degree of orientation (86%), compared to the single-scale substrate (W0.3 and W26), indicating that the hierarchical structure with parallel combination enhanced the orientation of hBM-MSCs. In contrast, cells on the W0.3⊥26 showed irregular morphology and less degree of orientation (34%), suggesting that the perpendicular combination suppressed the orientation.

In addition, we have also quantified the average single cell area by actin staining. Figure 6C displays that hBM-MSCs on Flat and W0.3 substrate exhibited the largest cell area (1746 µm$^2$). In contrast, the cell area was much lower for W26, W0.3∥26, and W0.3⊥26 (1204, 597, and 791 µm$^2$, respectively). These findings suggest that hierarchical substrates with different directions have a significant influence on the macroscopic behavior of hBM-MSCs.

The neuron differentiation on different hierarchical substrates was examined by immunofluorescent staining similar as performed on the topography gradient. The immunostaining results (**Figure 7**A) for Tuj1 and MAP2 after 14 d of culturing cells in differentiation medium showed that neurogenesis was significantly upregulated for cells cultured on the W0.3∥26, compared with all other anisotropic structures and the Flat control. Quantification of these results (Figure 7B,C) corroborated this observation, displaying that the neurogenesis degree of hBM-MSCs for W0.3, W26, W0.3∥26 and W0.3⊥26 were 15, 26, 37, 23 times higher than that on the Flat substrate, respectively. The absolute outcomes between homogeneous wrinkle features such as W26 and those of the same size within the gradient approach display a slightly different behavior. This differences most likely occurs because the area of investigation within the gradient contains a mix of sizes (W26 is an average), influences of cell–cell communication (paracrine and physical contact) under different stimulation on the gradient. Therefore, it is pertinent to include correct controls and care needs to be taken to interpret results. Interestingly, for the hierarchical structure, the differentiation for cells grown on W0.3∥26 was more efficient than that on W0.3⊥26, indicating that the design where the nanotopography direction was parallel with the microstructures, resembling the assembled nerve fibers, exhibited the highest degree of neurogenesis. Taken together, these results demonstrate that the hierarchical structure containing microsized and nanosized wrinkles have a combined positive effect on the neuron fate commitment of hBM-MSCs as long as the orientation of the structure is chosen appropriately.

## 2.4. Neural Differentiation Mediated by Cell Contractility and YAP–TAZ Signal

The combined enhancement of the neurogenesis in the multiscale substrate led us to explore the reason why the hierarchical structure showed the enhanced neurogenesis in comparison to the single-scale substrate. For this purpose, cell contractility or tension was characterized by phosphorylated myosins. In our study, immunofluorescent staining of phosphorylated myosin light chain (pMLC) was performed for hMSCs after 24 h culture. Representative fluorescence images of MSCs stained with pMLC are displayed in **Figure 8**. Interestingly, cells cultured on Flat and W0.3 were found to have higher levels of pMLC expression compared to W26 and hierarchical substrates. Quantitative results showed that the level of pMLC of the cells on Flat and W0.3 were 5.9 and 4.6-fold of that on the W0.3∥26, respectively. However, there is no significant difference between W26, W0.3∥26, and W0.3⊥26. These results indicate that the larger wrinkles have an important influence on the cell contractility and that hierarchical structures with the larger winkle structure as a feature do not alter the contractility.

In addition to cell tension, YAP–TAZ (transcription coactivator with PDZ-binding motif, also known as WWTR1) localization was also investigated (**Figure 9**). Paralogous coactivators Yorkie-homologues YAP and TAZ have been identified as a mechanical rheostat of the cell.[50] The functionality of YAP–TAZ can be regulated by biophysical stimuli. When the cytoskeletal tension is generated, YAP–TAZ localizes into the
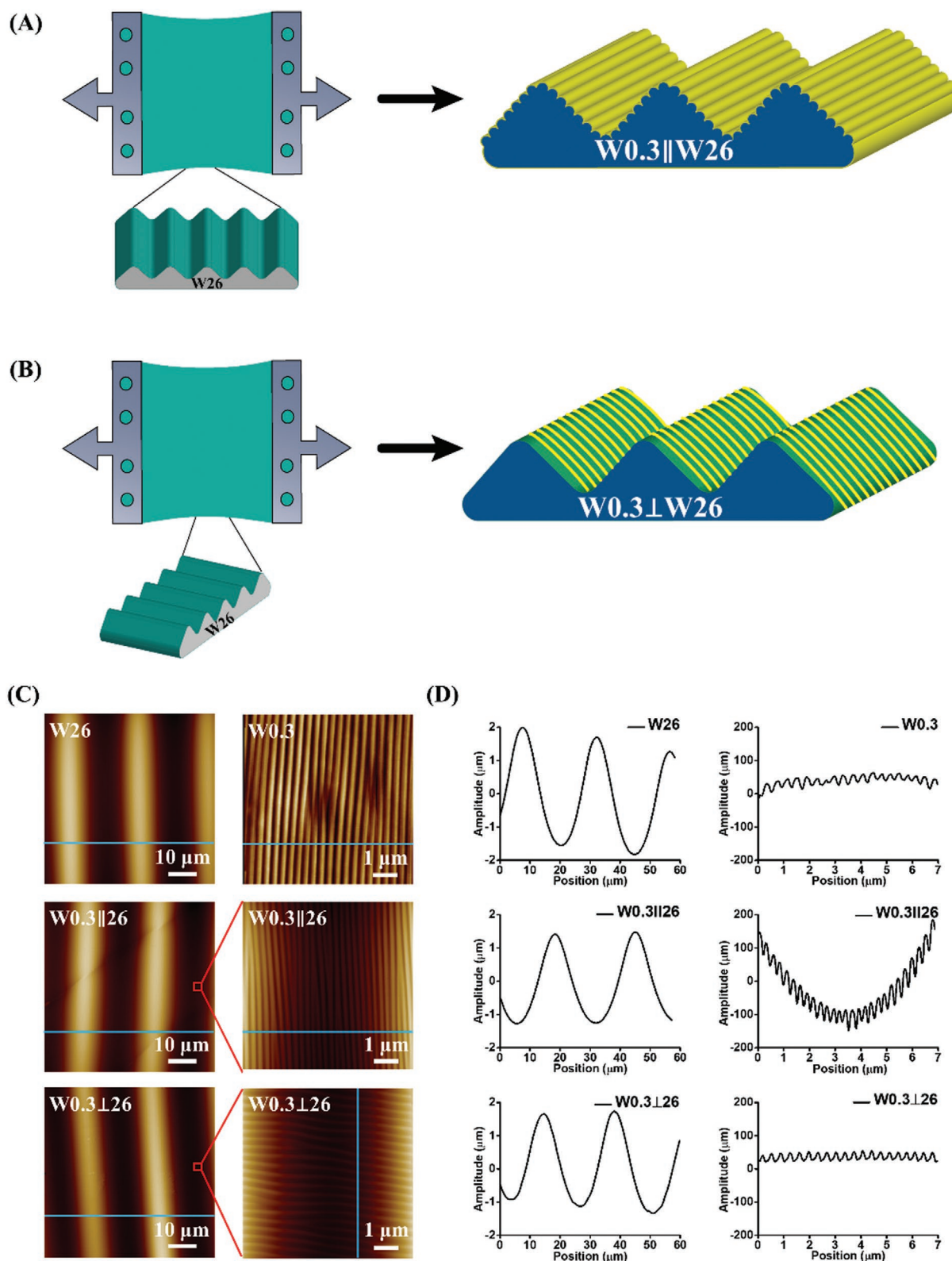
**ADVANCED
SCIENCE NEWS**

www.advancedsciencenews.com

**ADVANCED
HEALTHCARE
MATERIALS**

www.advhealthmat.de

**Figure 5.** Preparation of the hierarchical substrates. A) When the stretch direction is parallel to the wrinkle, W0.3‖W26 is fabricated. B) When the stretch direction is perpendicular to the wrinkle, W0.3⊥W26 is formed. C) AFM images and D) height profiles of the structured PDMS surfaces obtained after imprinting. The colored lines stand for the position from AFM image to draw the height profiles. Scale bar is 10 µm for the lower magnification image and 1 µm for the higher magnification image.
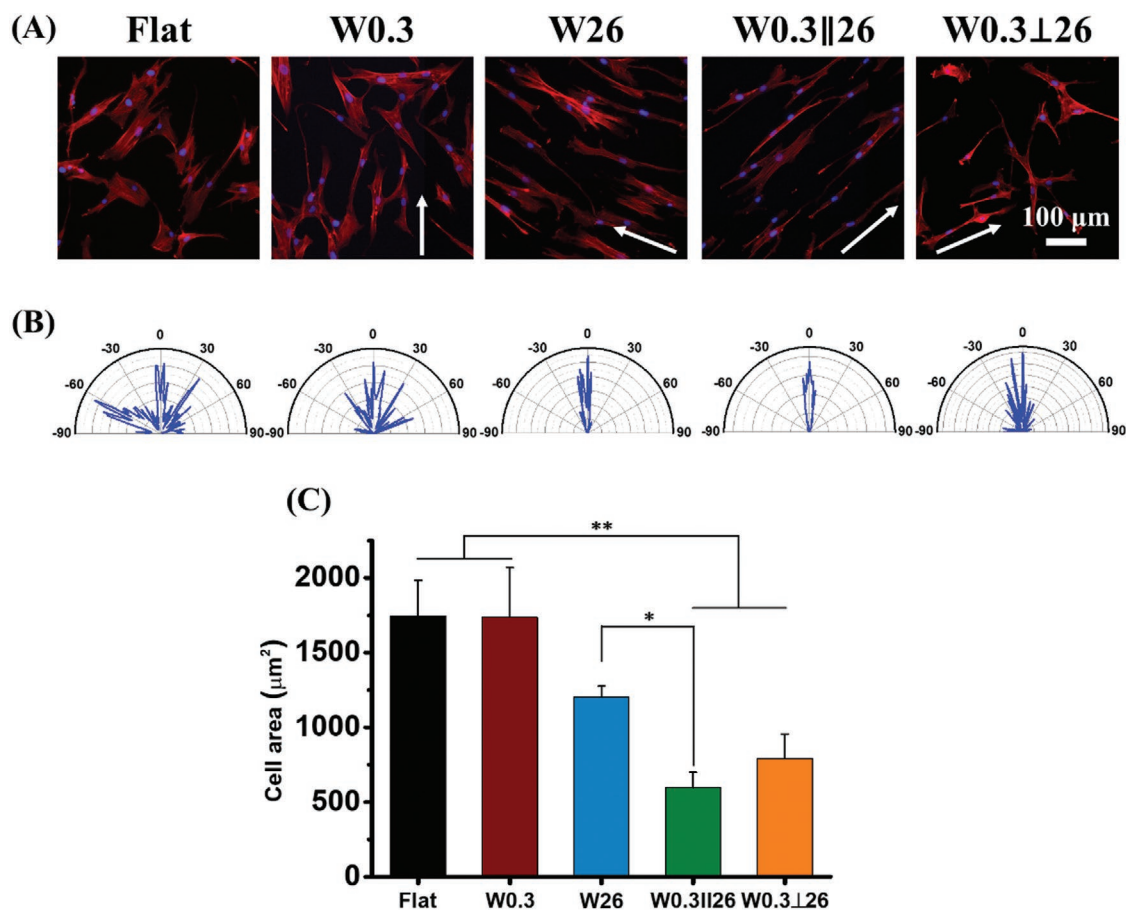
**Figure 6.** Influence of hierarchical substrates on the morphology of hBM-MSCs cultured for 1 day. A) Representative fluorescence microscopy images of hBM-MSCs grown on different topographies. Cell cytoskeleton and cell nucleus were stained with TRITC-labeled phalloidin (red) and by DAPI (blue), respectively. The white arrow indicates the direction of (larger) wrinkle. Scale bar on the gradients represents 100 μm. B) Corresponding angular histograms of cell cytoskeleton angles from results in (A). C) Histogram of the statistical results of the cell area. Data are shown as mean ± standard deviation (SD), and *$P < 0.05$, **$P < 0.01$. Each experiment was performed in triplicate.

nucleus, modulating gene expression. However, when tension is interrupted, they are sequestered in the cytoplasm and their activity is reduced.[50]

After 1 d culture, the cells were immunofluorescently stained to show the YAP–TAZ localization. Interestingly, when cells grown on the Flat and W0.3, YAP–TAZ display a higher translocation into cell nucleus. In contrast, W26 and hierarchical structure led to cytoplasmic YAP–TAZ. Quantitative analysis indicated that about 41% and 28% of cells grown on Flat and W0.3 exhibited nuclear localization, respectively. Alternatively, only about 5% of cells showed nuclear localization for W26, W0.3‖26 and W0.5⊥26. However, there was no significant difference between the two hierarchical substrates. Taken together, these results demonstrate that the promoted neurogenesis of hBM-MSCs on W0.3‖26 is mediated by cell tension and YAP–TAZ pathway.

## 3. Discussion

While it has been well established that surfaces with anisotropic topography have an important influence on cellular activity including cell motility, proliferation, and differentiation, there is still a lack of profound knowledge on specific parameters that are optimum to enhance the desired cell behavior, especially for neuron differentiation. Nevertheless, although previous studies focused on the neurogenesis through independent substrates with arbitrarily selected parameters, it provided interesting but limited information. In our study, the PDMS wrinkle gradient was fabricated to define the surface properties that promote neuron differentiation of hBM-MSCs. The wrinkle gradient was produced via a convenient stretch-plasma oxidation-release process. After immunofluorescent staining of different markers (Tuj1 and MAP2), the wrinkle gradient platform with different wavelengths and amplitudes could screen and output the optimum wrinkle feature for neurogenesis of hBM-MSCs. To the best of our knowledge, this is the first time to systematically investigate neuron differentiation of stem cells in a high-throughput screening manner.

It is generally known that hierarchical structures consisting of both micro- and nanoscale structures enable the effective regulation of stem cell differentiation by controlling the cytoskeleton orientation and intracellular focal adhesion protein assembly.[51] Several studies have focused on the effect of hierarchical structure on neuron fate lineage of stem cells.[32,33] For
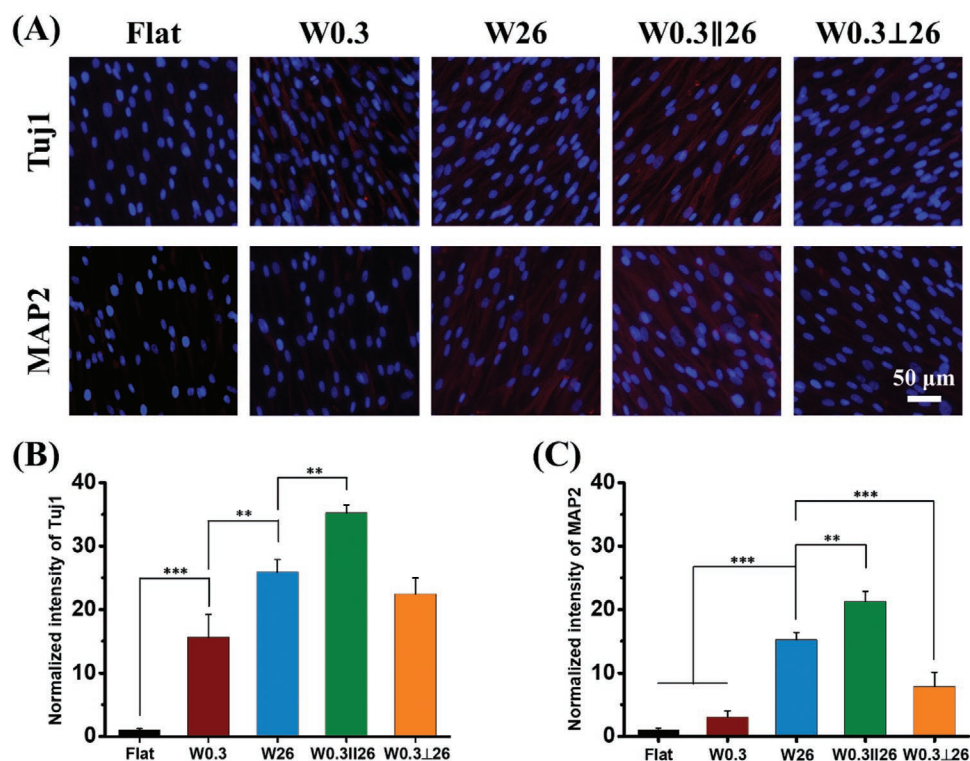
**Figure 7.** Immunofluorescence staining of neural marker Tuj1 and MAP2 of cells cultured in neuronal induction medium (IM) for 14 d. A) Cells were stained for DAPI (nucleus, blue), Tuj1 (red), and MAP2 (red), respectively. Scale bar is 50 µm. Quantified expression of B) Tuj1 and C) MAP2 of cells cultured in single and double scales substrates normalized by Flat surface. Data are shown as mean ± standard deviation (SD), and **$P < 0.01$, ***$P < 0.001$. Each experiment was performed in triplicate.

instance, Im and co-workers fabricated the hierarchical wrinkle structures for investigating the fate commitment of human neural stem cells, and found multiscale wrinkle (wavelengths 100 nm and 1.4 µm, parallel with each other) enhanced neurogenesis.[49] However, they did not compare the discrepancy between differently integrated type (for example, parallel versus perpendicular). In our study, we examined the potential for stem cell neurogenesis cultured on hierarchical structure based on the results of screening. Moreover, the influence of different directions of hierarchical structure (W0.3∥26 and W0.3⊥26) on neuron differentiation was also investigated. From the results of Tuj1 and MAP2 staining, it could be observed that W0.3∥26 could significantly enhanced the neurogenesis in comparison to single scale substrates (W0.3, W26) and W0.3⊥26. These results suggest that the style of integration for the hierarchical structure is important for neuron differentiation of hBM-MSCs.

Several studies have demonstrated that neurogenesis of stem cells is mediated by YAP. Particularly, Kiessling and co-workers[52] have reported that compliant substrata inhibited the nuclear localization of YAP by adding a small molecule (latrunculin A, inhibitor of F-actin polymerization) and promoted highly efficient differentiation of human pluripotent stem cells into postmitotic neurons. Im and co-workers[49] have also demonstrated that restricted activation of RhoA of human neural stem cells promoted cytoplasmic localization of YAP, and this is highly associated with enhanced neurogenesis. Furthermore, Yim and co-workers[53] showed that the essential role of

actomyosin contractility in topography-induced neuron differentiation of hMSCs. Our results are consistent with their findings. In this study, we have shown that YAP/TAZ is involved in a regulatory mechanism by which substrates with hierarchical structure direct hBM-MSCs toward the neuron lineage by decreasing the nuclear localization of YAP/TAZ. We have further demonstrated that the decreased nuclear localization of YAP/TAZ is mediated by the lower cell contractility, thus downregulating neurogenesis of hBM-MSC. The potential mechanism for different degrees of neurogenesis of hBMSCs on W0.3∥26 and Flat substrate mediated by cell contractility and YAP/TAZ signaling pathway is illustrated in **Figure 10**. Nevertheless, the cells on parallel (W0.3∥W26) and perpendicular structures (W0.3⊥W26) displayed similar differences in YAP/TAZ nuclear localization and myosin formation, the perpendicular substrate did not show the similar level of neuron differentiation compared with the parallel sample. This disparity is likely attributable to other signal pathway related with neuron differentiation, for instance, Wnt/$\beta$-catenin signaling,[54] and $\beta$1 integrin/mitogen-activated protein kinase (MAPK) pathway.[55] Therefore, further investigation is necessary to fully elucidate the mechanism about neuron differentiation stimulated by hierarchical substrates.

## 4. Conclusion

In this study, a high-throughput screening platform with wrinkle gradient was fabricated (amplitudes from 541 to

**ADVANCED**
**SCIENCE NEWS**
www.advancedsciencenews.com

**ADVANCED**
**HEALTHCARE**
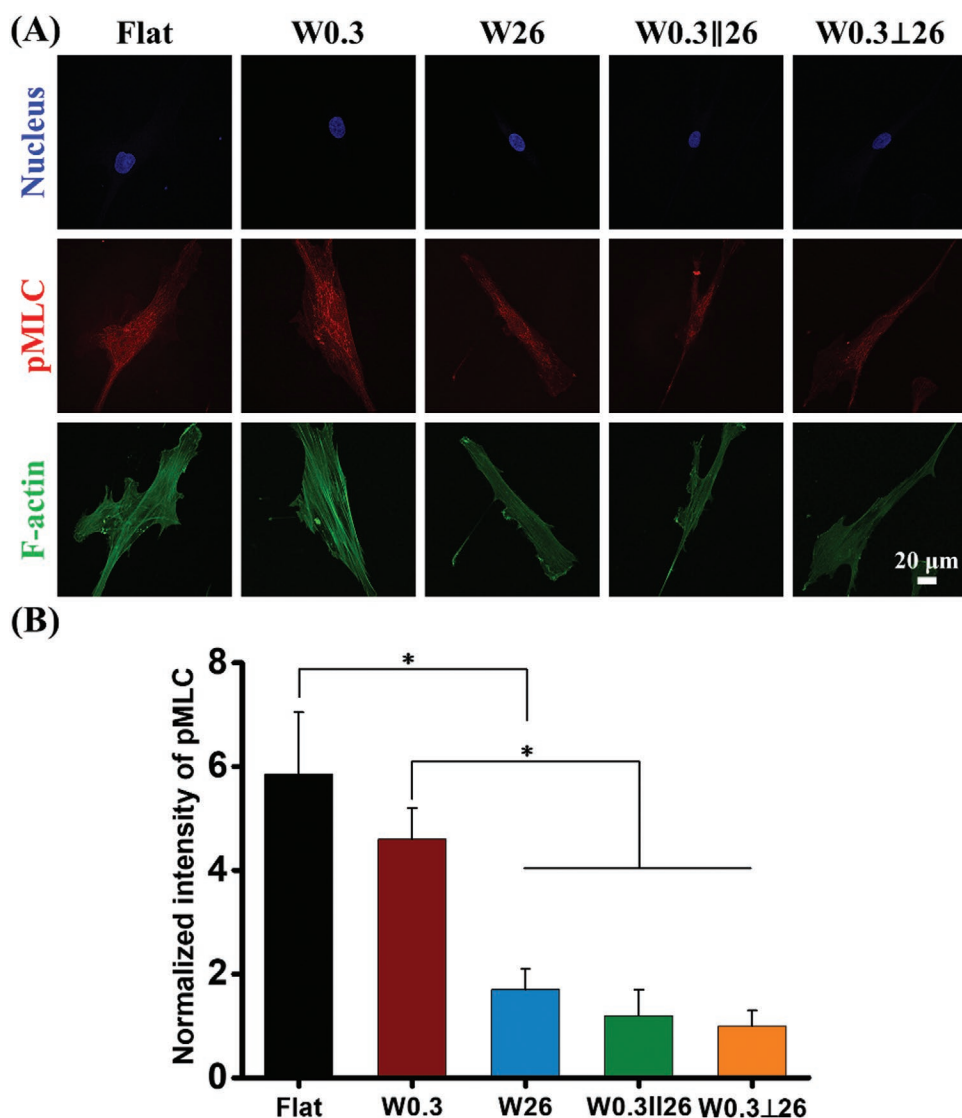**MATERIALS**
www.advhealthmat.de

**Figure 8.** Fluorescent indication of cell tension on hierarchical structure substrates. A) Typical fluorescence image of single stem cells on the indicated surfaces cultured in the growth medium for 24 h. Blue: nucleus, Red: pMLC, Green: F-actin. Scale bar represents 20 µm. B) Integrated fluorescence intensity of pMLC, and normalized by W0.3⊥26 substrate. Data are shown as mean ± standard deviation (SD) ($n \geq 20$ cells), and $*P < 0.05$. Each experiment was performed in triplicate.

3073 nm and wavelengths between 4 and 30 µm) and the optimal parameter for directing hBM-MSCs toward the neuron lineage was found (W: 26.7 µm; A: 2.89 µm). Furthermore, the hierarchical structure (W3‖W26) could significantly enhance the neural differentiation, compared to the single scale topography. Moreover, this process is associated with the lower percentage of nucleus localization of YAP/TAZ and weaker cell tension. This study has great potential in designing neuron-inductive materials and highlights the importance of the hierarchical structure for directing stem cells toward neurogenesis. Additionally, the understanding of interactions between stem cells and topography will facilitate further clinical applications of topography-mediated stem cell neurogenesis in tissue engineering and regenerative medicine.

## 5. Experimental Section

*PDMS Preparation and Wrinkle Gradient Formation*: PDMS film was prepared as described previously.[38] Briefly, PDMS precursor was mixed with cross-linker (Sylgard 184, Dow Corning) in a ratio of 15:1 by weight. The mixtures were vigorously stirred with a spatula, degassed under vacuum for 15 min to remove the air bubbles completely, and deposited onto cleaned 12 × 12 cm squared polystyrene Petri dish. The poured PDMS was cured at 70 °C overnight. After curing, the elastomer film was cut into the desired dimension.

PDMS substrates with wrinkle gradient were prepared as described previously. For the wrinkled gradient with $SiO_2$ surface, the PDMS membrane was placed in a custom-made stretching apparatus and stretched uniaxial by 10% of the original length. Stretched PDMS was partly covered with a right angled triangular prism mask (1.3 cm) and oxidized in air plasma under the stable pressure (Plasma Activate Flecto 10 USB, maximum intensity). After oxidation, the strain was released, which induced wrinkle gradient formation with different wavelengths and
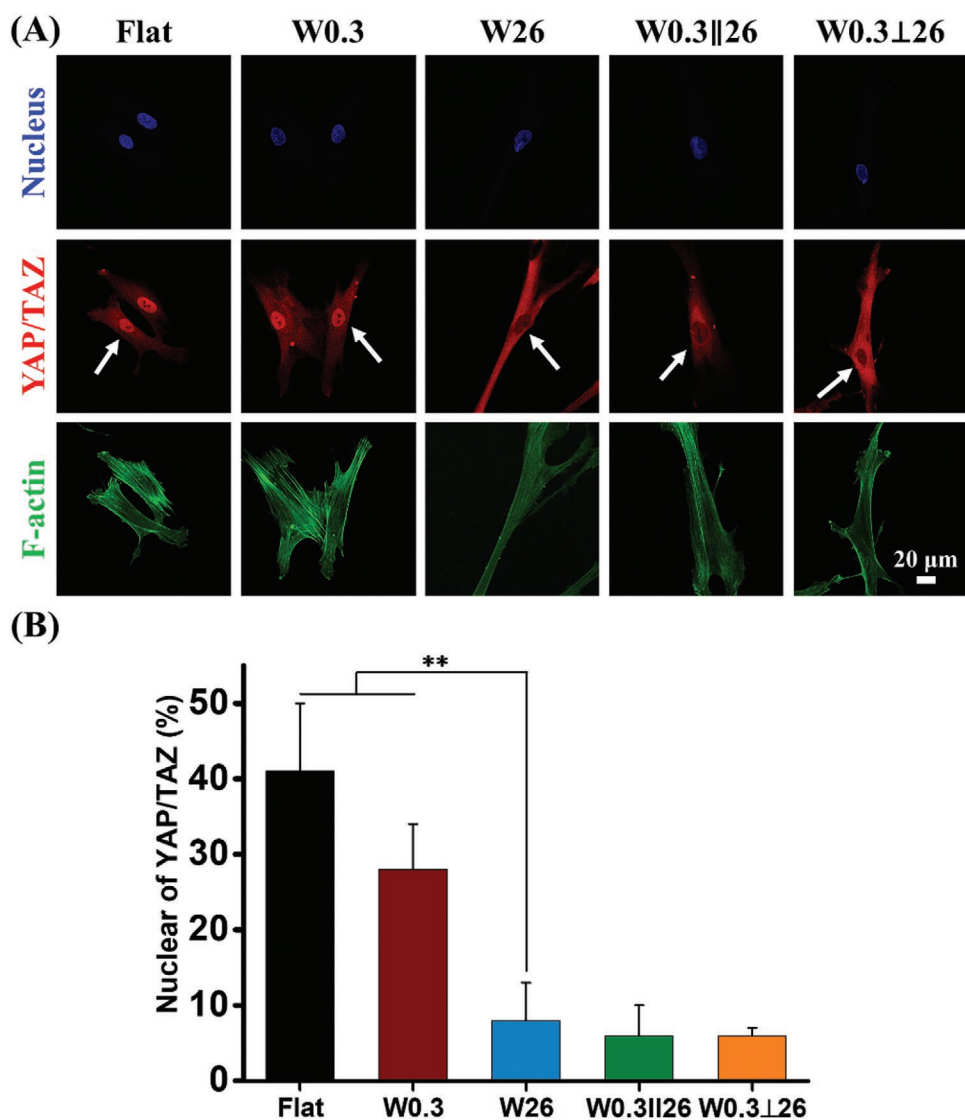
**Figure 9.** Representative images of YAP/TAZ localization in hBM-MSCs seeded onto different surfaces for 24 h. Blue: nucleus, Red: YAP/TAZ, Green: F-actin. The white color arrows refer to the YAP/TAZ located in the nucleus position or not. Scale bar represents 20 μm. B) The number of cells with nuclear localization of YAP/TAZ. Data are shown as mean ± standard deviation (SD) ($n = 100$ cells), and **$P < 0.01$. Each experiment was performed in triplicate.

amplitudes. PDMS wrinkle gradient was applied as molds on which a fresh mixture of elastomer base/cross-linker (10:1) was poured, followed by curing at 70 °C overnight. After that, the molds were removed and the freshly prepared PDMS substrates with wrinkle gradient were additionally treated with air plasma at 500 mTorr for 1 min and used for cell seeding. This imprinting approach led to the same surface chemistry and mechanical properties on PDMS wrinkle gradient.

*Preparation of Single-Scale Structure and Hierarchical Architecture*: The single scale anisotropic substrates (wavelength: 0.3 μm, 26 μm) were prepared as described previously.[56] For the preparation of the anisotropic wrinkle structure, the conditions are summarized in **Table 1**. The different surface topographies are named as Flat, W0.3, and W26. For the fabrication of the hierarchical wrinkle structure, the imprinted W26 substrate (10:1 prepolymer:cross-linker) was used as a new substrate, which is suitable to perform the stretch-plasma oxidation-release process for incorporating W0.3 on the top of W26 substrate. Importantly, the stretch direction could be varied with respect to the direction of the first substrate, and thereby the double-scale hierarchical structure was fabricated with a variation in the topography direction.

Here substrates with parallel direction (W0.3∥W26) and perpendicular direction (W0.3⊥W26) were fabricated and were subsequently named as W0.3∥26 and W0.3⊥26, respectively. To keep the same surface chemistry and mechanical properties, single scale and hierarchical substrates were performed the same imprinting process and treated with air plasma at 500 mTorr for 1 min for cell seeding.

*PDMS Surface Characterization*: AFM images were obtained by atomic force microscope (Nanoscope V Dimension 3100 microscope, Veeco, United States) operating with the tapping mode in air (model DNP-10 tip). To determine the wavelength and amplitude of the topographies, the obtained AFM images were analyzed using NanoScope Analysis software.

*Cell Culture*: hBM-MSCs obtained from Lonza were used for the experiments. hBM-MSCs were cultured in growth medium composed of Alpha modified Eagle medium (Gibco), 10% (v/v) fetal bovine serum (Gibco), 0.1% ascorbic acid 2-phosphate (Sigma) and 1% penicillin/streptomycin (Gibco). Cells from three different batches were mixed to account for donor heterogeneity and were incubated in T75 culture flasks at 37 °C in a humidified atmosphere with 5% $CO_2$. The culture medium
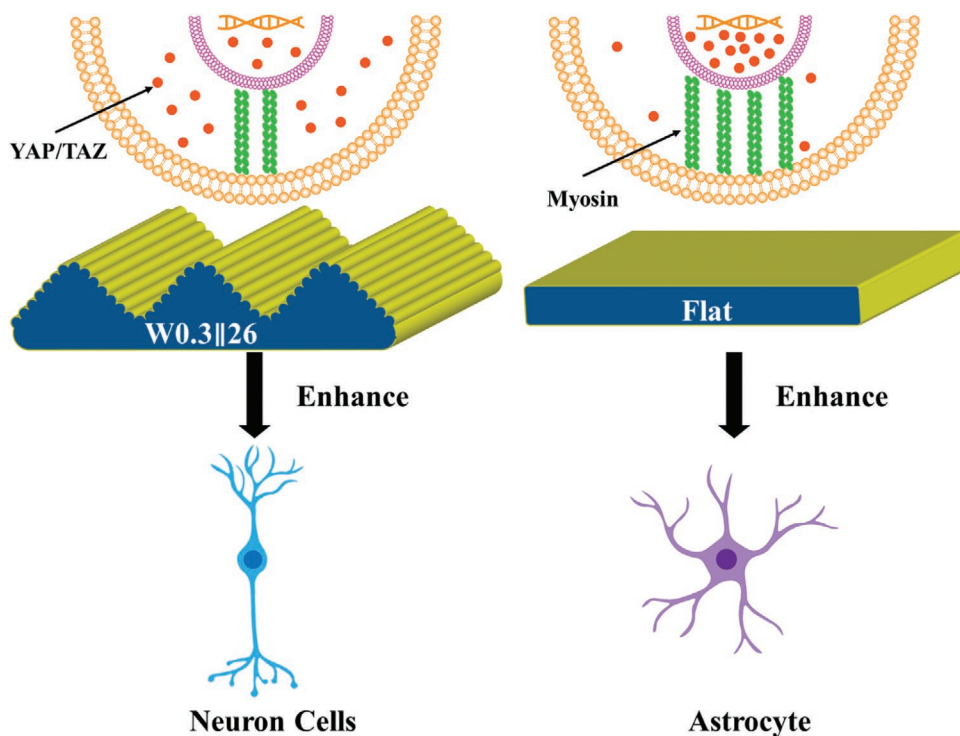
**Figure 10.** Schematic showing the reverse effect of hierarchical wrinkle structure and Flat surface for directing neurogenesis. Hierarchical substrates will diminish the cell contractility, which results in the localization of YAP/TAZ into cytoplasm, therefore improve neuron differentiation of hBM-MSCs. Flat substrate increases cell tension, and results in the translocation of YAP–TAZ to the nucleus, thus facilitating the differentiation of stem cells into astrocytes.

was changed every 3 d and cells were harvested at ≈80% confluency. MSCs of passage 4 were used for all of the experiments.

*Neuronal Differentiation*: All of the wrinkle substrates were first cleaned with 70% ethanol for 2 min and washed three times with Dulbecco's phosphate-buffered saline (D-PBS) solution. Then, hBM-MSCs were seeded onto the wrinkled substrate at a seeding density of $1.0 \times 10^4$ cells per well in 24 well plates. To induce neuronal differentiation the growth medium was replaced with neuronal induction medium (IM) composed of growth medium supplemented with 20 ng mL$^{-1}$ basic fibroblast growth factor (bFGF, Peprotech), 10 ng mL$^{-1}$ human nerve growth factor ($\beta$-NGF, Peprotech), 10 ng mL$^{-1}$ human brain-derived neurotrophic factor (bDNF, Peprotech) and 2% B27 (Gibco). The culture medium was changed every 3 d. The Flat PDMS served as a control.

*Immunofluorescence Staining and Imaging*: At the end of cell culturing time point, the cells on PDMS scaffolds were fixed in 3.7% paraformaldehyde (Sigma) for 20 min and subsequently permeabilized with 0.5% Triton X-100 (Sigma) for 3 min. The samples were blocked with 5% bovine serum albumin (Sigma) in PBS solution for 30 min and incubated with primary antibody solution and later with secondary

antibody solution for 1 h, respectively. The primary antibodies with their respective optimized concentrations were: mouse anti-$\beta$-tubulin III (Tuj1) antibody (1:100, Santa Cruze); mouse antimicrotubule associated protein 2 (MAP2) antibody (Santa Cruze, 1:50); mouse antiglial fibrillary acidic protein (GFAP) antibody (Santa Cruze, 1:50), YAP–TAZ (Santa Cruz Biotechnology, SC-101199, 1:100), pMLC (Cell Signaling, #3675, 1:100). The secondary antibody was Rhodamine Red-X labeled goat-anti-mouse antibody (Jackson Immunolab, 1:100). Nuclei and fiber actin were stained with DAPI (Invitrogen, 1:100) and FITC/TRITC-phalloidin (Sigma, 1:100), respectively, by incubation for 1 h. Finally, the cells were imaged with TissueFaxs, with a Zeiss AxioImager Z1Microscope System (Tissue-Gnostics GmbH, Vienna, Austria) at 10× magnification. Myosin and YAP staining was observed using a LEICA TCS SP2 CLSM equipped with a 40 × NA 0.80 water immersion objective. The cell area was analyzed by Tissue Quest software (high-throughput analysis technique) via fluorescent F-actin stained cells. Analysis for cell orientation was conducted with Fiji using the Orientation J plug-in, and for cell area and cell orientation, at least 200 cells were taken into consideration for each substrate. The expression of Tuj1, MAP2 and GFAP was evaluated quantitatively by determining the fluorescence output measured by Fiji software, and then normalized to cell number, determined by nucleus staining with DAPI, and then quantitatively analyze via the TissueQuest software (high-throughput analysis technique). The fluorescent intensity of myosin was quantified as described previously.[57]

*Statistics Analysis*: All data points are expressed as mean values ± standard deviation. Statistical analysis was performed with Origin 9.0 software. All data were analyzed using one-way analysis of variance (ANOVA) with Tukey's test to determine differences between groups. A value of $p < 0.05$ was considered to be statistically significant.

**Table 1.** Conditions for PDMS substrates (molds) with different wrinkle parameters.

| Substrate[a] | Ratio of prepolymer and crosslinker | Stretched percent [%] | Operating pressure [Torr] | Plasma time [s] |
|---|---|---|---|---|
| Flat | 10:1 | – | – | – |
| W0.3/A0.02 | 10:1 | 30 | 14 | 40 |
| W26/A2.9 | 15:1 | 10 | 0.025 | 1800 |

[a]W and A are the abbreviation of wavelength and amplitude, respectively, and the unit for W and A is µm. The different surface topographies are further reported as Flat, W0.3, and W26.

## Supporting Information

Supporting Information is available from the Wiley Online Library or from the author.

[1] P. Assinck, G. J. Duncan, B. J. Hilton, J. R. Plemel, W. Tetzlaff, *Nat. Neurosci.* **2017**, *20*, 637.

[2] B. Zhang, Y. Yan, Y. Zhu, W. Yang, W. Le, B. Chen, R. Zhu, L. Cheng, *Adv. Mater.* **2018**, *30*, 1705694.

[3] T. C. Tseng, L. Tao, F. Y. Hsieh, Y. Wei, I. M. Chiu, S. H. Hsu, *Adv. Mater.* **2015**, *27*, 3518.

[4] L. Gong, L. Cao, Z. Shen, L. Shao, S. Gao, C. Zhang, J. Lu, W. Li, *Adv. Mater.* **2018**, *30*, 1705684.

[5] G. Orive, E. Anitua, J. L. Pedraz, D. F. Emerich, *Nat. Rev. Neurosci.* **2009**, *10*, 682.

[6] O. Lindvall, Z. Kokaia, A. Martinez-Serrano, *Nat. Med.* **2004**, *10*, S42.

[7] J. Fiedler, B. Özdemir, J. Bartholomä, A. Plettl, R. E. Brenner, P. Ziemann, *Biomaterials* **2013**, *34*, 8851.

[8] G. Abagnale, M. Steger, V. H. Nguyen, N. Hersch, A. Sechi, S. Joussen, B. Denecke, R. Merkel, B. Hoffmann, A. Dreser, U. Schnakenberg, A. Gillner, W. Wagner, *Biomaterials* **2015**, *61*, 316.

[9] Y. N. Wu, J. B. K. Law, A. Y. He, H. Y. Low, J. H. P. Hui, C. T. Lim, Z. Yang, E. H. Lee, *Nanomed.: Nanotechnol., Biol. Med.* **2014**, *10*, 1507.

[10] X. Zhang, X. Cui, D. Wang, S. Wang, Z. Liu, G. Zhao, Y. Zhang, Z. Li, Z. L. Wang, L. Li, *Adv. Funct. Mater.* **2019**, *29*, 1900372

[11] A. Trounson, C. McDonald, *Cell Stem Cell* **2015**, *17*, 11.

[12] M. Poudineh, Z. Wang, M. Labib, M. Ahmadi, L. Zhang, J. Das, S. U. Ahmed, S. Angers, S. O. Kelley, *Nano Lett.* **2018**, *18*, 7188.

[13] J. Kim, J. R. Staunton, K. Tanner, *Adv. Mater.* **2016**, *28*, 132.

[14] J. H. Kim, H. W. Kim, K. J. Cha, J. Han, Y. J. Jang, D. S. Kim, J.-H. Kim, *ACS Nano* **2016**, *10*, 3342.

[15] T. C. Von Erlach, S. Bertazzo, M. A. Wozniak, C. M. Horejs, S. A. Maynard, S. Attwood, B. K. Robinson, H. Autefage, C. Kallepitis, A. Del Río Hernández, C. S. Chen, S. Goldoni, M. M. Stevens, *Nat. Mater.* **2018**, *17*, 237.

[16] M. J. Dalby, N. Gadegaard, R. O. C. Oreffo, *Nat. Mater.* **2014**, *13*, 558.

[17] D. Jain, S. Mattiassi, E. Goh, E. Yim, *Neural Regener. Res.* **2020**, *15*, 573.

[18] C. Simitzi, K. Karali, A. Ranella, E. Stratakis, *ChemPhysChem* **2018**, *19*, 1143.

[19] G. J. Her, H. C. Wu, M. H. Chen, M. Y. Chen, S. C. Chang, T. W. Wang, *Acta Biomater.* **2013**, *9*, 5170.

[20] K. H. Vining, D. J. Mooney, *Nat. Rev. Mol. Cell Biol.* **2017**, *18*, 728.

[21] N. D. Leipzig, M. S. Shoichet, *Biomaterials* **2009**, *30*, 6867.

[22] E. E. Charrier, K. Pogoda, R. G. Wells, P. A. Janmey, *Nat. Commun.* **2018**, *9*, 449.

[23] J. Du, X. Chen, X. Liang, G. Zhang, J. Xu, L. He, Q. Zhan, X. Q. Feng, S. Chien, C. Yang, *Proc. Natl. Acad. Sci. USA* **2011**, *108*, 9466.

[24] A. J. Engler, S. Sen, H. L. Sweeney, D. E. Discher, *Cell* **2006**, *126*, 677.

[25] W. Guo, X. Zhang, X. Yu, S. Wang, J. Qiu, W. Tang, L. Li, H. Liu, Z. L. Wang, *ACS Nano* **2016**, *10*, 5086.

[26] Y. Jin, J. Seo, J. S. Lee, S. Shin, H. J. Park, S. Min, E. Cheong, T. Lee, S. W. Cho, *Adv. Mater.* **2016**, *28*, 7365.

[27] J. Lee, A. A. Abdeen, D. Zhang, K. A. Kilian, *Biomaterials* **2013**, *34*, 8140.

[28] R. Ayala, C. Zhang, D. Yang, Y. Hwang, A. Aung, S. S. Shroff, F. T. Arce, R. Lal, G. Arya, S. Varghese, *Biomaterials* **2011**, *32*, 3700.

[29] J. Kim, H. N. Kim, K. T. Lim, Y. Kim, S. Pandey, P. Garg, Y. H. Choung, P. H. Choung, K. Y. Suh, J. H. Chung, *Biomaterials* **2013**, *34*, 7257.

[30] M. J. Dalby, M. O. Riehle, H. Johnstone, S. Affrossman, A. S. G. Curtis, *Cell Biol. Int.* **2004**, *28*, 229.

[31] G. A. Dunn, J. P. Heath, *Exp. Cell Res.* **1976**, *101*, 1.

[32] K. K. B. Tan, J. Y. Tann, S. R. Sathe, S. H. Goh, D. Ma, E. L. K. Goh, E. K. F. Yim, *Biomaterials* **2015**, *43*, 32.

[33] A. A. K. Moe, M. Suryana, G. Marcy, S. K. Lim, S. Ankam, J. Z. W. Goh, J. Jin, B. K. K. Teo, J. B. K. Law, H. Y. Low, E. L. K. Goh, M. P. Sheetz, E. K. F. Yim, *Small* **2012**, *8*, 3050.

[34] S. Ankam, M. Suryana, L. Y. Chan, A. A. K. Moe, B. K. K. Teo, J. B. K. Law, M. P. Sheetz, H. Y. Low, E. K. F. Yim, *Acta Biomater.* **2013**, *9*, 4535.

[35] F. Pan, M. Zhang, G. Wu, Y. Lai, B. Greber, H. R. Schöler, L. Chi, *Biomaterials* **2013**, *34*, 8131.

[36] J. Baek, W.-B. Jung, Y. Cho, E. Lee, G.-T. Yun, S.-Y. Cho, H.-T. Jung, S. G. Im, *ACS Appl. Mater. Interfaces* **2019**, *11*, 17247.

[37] S. Ankam, B. K. K. Teo, M. Kukumberg, E. K. F. Yim, *Organogenesis* **2013**, *9*, 128.

[38] Q. Zhou, O. Castañeda Ocampo, C. F. Guimarães, P. T. Kühn, T. G. Van Kooten, P. Van Rijn, *ACS Appl. Mater. Interfaces* **2017**, *9*, 31433.

[39] A. B. Faia-Torres, S. Guimond-Lischer, M. Rottmar, M. Charnley, T. Goren, K. Maniura-Weber, N. D. Spencer, R. L. Reis, M. Textor, N. M. Neves, *Biomaterials* **2014**, *35*, 9023.

[40] G. R. Liguori, Q. Zhou, T. T. A. Liguori, G. G. Barros, P. T. Kühn, L. F. P. Moreira, P. van Rijn, M. C. Harmsen, *Stem Cells Int.* **2019**, *2019*, 5387850.

[41] A. M. Almonacid Suarez, Q. Zhou, P. Van Rijn, M. C. Harmsen, *J. Tissue Eng. Regener. Med.* **2019**, *13*, 2234.

[42] G. Abagnale, A. Sechi, M. Steger, Q. Zhou, C. C. Kuo, G. Aydin, C. Schalla, G. Müller-Newen, M. Zenke, I. G. Costa, P. van Rijn, A. Gillner, W. Wagner, *Stem Cell Rep.* **2017**, *9*, 654.

[43] Q. Zhou, P. Wünnemann, P. T. Kühn, J. de Vries, M. Helmin, A. Böker, T. G. van Kooten, P. van Rijn, *Adv. Mater. Interfaces* **2016**, *3*, 1600275.

[44] Q. Zhou, Z. Zhao, Z. Zhou, G. Zhang, R. C. Chiechi, P. van Rijn, *Adv. Mater. Interfaces* **2018**, *5*, 1800334.

[45] M. P. Lutolf, P. M. Gilbert, H. M. Blau, *Nature* **2009**, *462*, 433.

[46] C. Y. Tay, H. Yu, M. Pal, W. S. Leong, N. S. Tan, K. W. Ng, D. T. Leong, L. P. Tan, *Exp. Cell Res.* **2010**, *316*, 1159.

[47] T. A. Petrie, J. E. Raynor, D. W. Dumbauld, T. T. Lee, S. Jagtap, K. L. Templeman, D. M. Collard, A. J. García, *Sci. Transl. Med.* **2010**, *2*, 45ra60.

[48] M. R. Lee, K. W. Kwon, H. Jung, H. N. Kim, K. Y. Suh, K. Kim, K. S. Kim, *Biomaterials* **2010**, *31*, 4360.

[49] J. Baek, S.-Y. Cho, H. Kang, H. Ahn, W.-B. Jung, Y. Cho, E. Lee, S.-W. Cho, H.-T. Jung, S. G. Im, *ACS Appl. Mater. Interfaces* **2018**, *10*, 33891.

[50] S. Dupont, L. Morsut, M. Aragona, E. Enzo, S. Giulitti, M. Cordenonsi, F. Zanconato, J. Le Digabel, M. Forcato, S. Bicciato, N. Elvassore, S. Piccolo, *Nature* **2011**, *474*, 179.

[51] K. Yang, H. Jung, H. R. Lee, J. S. Lee, S. R. Kim, K. Y. Song, E. Cheong, J. Bang, S. G. Im, S. W. Cho, *ACS Nano* **2014**, *8*, 7809.

[52] S. Musah, P. J. Wrighton, Y. Zaltsman, X. Zhong, S. Zorn, M. B. Parlato, C. Hsiao, S. P. Palecek, Q. Chang, W. L. Murphy, L. L. Kiessling, *Proc. Natl. Acad. Sci. USA* **2014**, *111*, 13805.

[53] B. K. K. Teo, S. T. Wong, C. K. Lim, T. Y. S. Kung, C. H. Yap, Y. Ramagopal, L. H. Romer, E. K. F. Yim, *ACS Nano* **2013**, *7*, 4785.

[54] X. Li, C. Fan, Z. Xiao, Y. Zhao, H. Zhang, J. Sun, Y. Zhuang, X. Wu, J. Shi, Y. Chen, J. Dai, *Biomaterials* **2018**, *183*, 114.

[55] Y. Wang, M. Yao, J. Zhou, W. Zheng, C. Zhou, D. Dong, Y. Liu, Z. Teng, Y. Jiang, G. Wei, X. Cui, *Biomaterials* **2011**, *32*, 6737.

[56] Q. Zhou, P. T. Kühn, T. Huisman, E. Nieboer, C. Van Zwol, T. G. Van Kooten, P. Van Rijn, *Sci. Rep.* **2015**, *5*, 16240.

[57] X. Liu, R. Liu, B. Cao, K. Ye, S. Li, Y. Gu, Z. Pan, J. Ding, *Biomaterials* **2016**, *111*, 27.

**2000117 (15 of 15)**